ChemPubSoc Europe

DOI: 10.1002/cctc.201600492

CHEMCATCHEM Full Papers

Ordered Mesoporous Materials as Supports for Stable Iron Catalysts in the Fischer–Tropsch Synthesis of Lower Olefins

Martin Oschatz,*[a] Wouter S. Lamme,[a] Jingxiu Xie,[a] A. Iulian Dugulan,[b] and Krijn P. de Jong*[a]

The Fe-catalyzed Fischer–Tropsch to olefins (FTO) synthesis is a non-oil-based route for the production of C_2–C_4 olefins. The understanding of the interplay between the catalytically active species, promoters, and support materials has improved over the last years, but the nanostructures of the various supports used are often not comparable. Several ordered mesoporous materials with a comparable pore size and pore symmetry are used as model supports for Fe-based FTO catalysts. Ammonium iron citrate is used as the Fe source for all supports, and Na and S are added as promoters. The formation of catalytically active iron carbide species is suppressed within the strongly interacting mesoporous silica support, but the weakly interacting carbon and silicon carbide supports yield highly active FTO catalysts. Carbon-supported catalysts show a high selectivity towards lower olefins, low methane production, and stable operation for up to 140 h under industrially relevant FTO conditions.

Introduction

Lower olefins (C_2–C_4) are crucial intermediates in the chemical industry and are produced traditionally by the steam cracking of naphtha or fluid catalytic cracking of vacuum gas oil. The Fischer–Tropsch to olefins (FTO) process is a non-oil-based alternative for the production of these compounds from synthesis gas (a mixture of CO and H_2).[1–3] Fe-based catalysts are applied in FTO because of their low methanation activity, high olefin/paraffin selectivity, resistance to contaminants, high water gas shift (WGS) activity, and low cost in comparison to Co catalysts.[4–10]

The catalytic properties of FTO catalysts can be enhanced by promoters such as alkali metals,[11,12] Cu,[13] Zn,[14] or V.[15] The addition of Na decreases the production of low-value methane, increases WGS activity, and facilitates the production of olefins instead of paraffins.[9,16] Traces of S reduce methane formation even more and increase the selectivity towards lower olefins because it restricts the termination of carbon-chain growth through hydrogenation, which thus favors the β-hydride abstraction pathway.[2,8,17] However, the interplay between catalytic properties, promoter effects, and Fe particle size is not well understood so far. Model catalysts[18,19] and operando methods[20] are increasingly applied to gain profound insights into the mechanisms of the FTO process.

To achieve the sufficient stability of FTO catalysts, the Fe particles are often supported on inorganic substrates to avoid particle growth and mechanical breakdown.[1] Porous silica,[9,21] alumina,[2] and carbon nanostructures[3,22,23] are the supports studied most widely. In addition to the chemical properties, the pore size, pore geometry, and pore connectivity have a significant influence on the size and dispersion of the catalyst nanoparticles.[21] However, the textures of various support materials are not easily compared, which complicates the interpretation of the structure–performance relationships.

Ordered mesoporous substrates are support structures for well-defined Fe and Co Fischer–Tropsch model catalysts because of their long-range ordered pore structure with a high symmetry and narrow pore size distribution (PSD).[9,24–26] We apply ordered mesoporous silica (SBA-15),[27] ordered mesoporous carbon (CMK-3),[28] and ordered mesoporous silicon carbide (OM-SiC),[29] which have comparable textural properties but different chemical compositions, as supports for Fe-based FTO catalysts with iron citrate as the precursor salt with and without Na and S as promoters. On one hand, the different chemical properties of the support material cause multiple effects on the structure of the catalyst (i.e., the Fe phases present and the Fe particle size during their preparation). On the other hand, with the use of ordered mesoporous supports, the catalytic performance can be interpreted straightforwardly. Although this work does not present fundamentally new concepts in catalyst preparation, the use of different ordered mesoporous supports helps us to gain a profound understanding of the synthesis–structure and structure–performance relation-

[a] Dr. M. Oschatz, W. S. Lamme, J. Xie, Prof. Dr. K. P. de Jong
Inorganic Chemistry and Catalysis
Debye Institute for Nanomaterials Science
Utrecht University
Universiteitsweg 99, 3584 CG Utrecht (The Netherlands)
E-mail: M.Oschatz@uu.nl
K.P.deJong@uu.nl

[b] Dr. A. I. Dugulan
Fundamental Aspects of Materials and Energy Group
Delft University of Technology
Mekelweg 15, 2629 JB Delft (The Netherlands)

Supporting information for this article can be found under http://dx.doi.org/10.1002/cctc.201600492.

ships, especially in the presence of Na/S promoters. Furthermore, the variation of the amount of S in the carbon-supported FTO catalyst represents an attempt towards catalyst optimization. The stability of these catalysts is increased by the encapsulation of Fe in the ordered mesopore system compared to a support with larger and disordered mesopores.

Results and Discussion

N_2 physisorption analyses of the pristine supports (Figure S1 and Table S1) show characteristic hysteresis loops because of their mesoporous structure. The average pore size of SBA-15, CMK-3, and OM-SiC is 8.8, 4.4, and 3.8 nm, respectively. In agreement with previous studies,[30,31] the contribution of micropores to the total pore volume is low. Although there are differences in the pore wall geometry (convex vs. concave surface curvature), these ordered mesoporous materials are suitable for the comparison of the influence of the chemical composition of the support material on the properties of Fe-based FTO catalysts because they are all high-surface-area supports with pores of comparable size and orientation.

Inductively coupled plasma optical emission spectroscopy (ICP-OES) of the calcined catalysts (Table S2) shows that the Fe content in all catalysts is slightly lower than expected theoretically, most likely because of the ill-defined stoichiometry of the precursors or the presence of traces of water.[32] In comparison to previous studies by our group,[8,10] a more than three-times higher Na/Fe ratio was chosen because of the much higher specific surface areas of the supports investigated in this work and their potential to bind Na extensively.

TEM investigations of the calcined catalysts show that well-dispersed Fe nanoparticles are encapsulated within the pore system of CMK-3 (Figure 1 A–C). The diameter of the particles (5.58 ± 1.22 nm) is in good agreement with the pore diameter of the carbon support (Figure S2 A). Fe particles are also well dispersed within the pore structure of OM-SiC, but larger agglomerates are also present on the external surface of the particles, most likely caused by the lower internal pore volume of this material in comparison to that of CMK-3 (Figure 1 D and E and Figure S2 B). No particles are embedded in the pore system of SBA-15 because the thermal treatment of iron citrate/silica leads to the formation of an iron silicate layer on the surface of the SBA-15 as reported previously for other SiO_2 supports that interact strongly with Fe.[33]

XRD measurements after calcination show the presence of Fe_2O_3 in the pore systems of CMK-3 and OM-SiC (Figure S3). For both supports, the promoters are detected partly as sodium sulfide. Independent of the presence of promoters, no crystalline Fe species are detected in case of the SBA-15 support because of the formation of iron silicate in the amorphous support pore walls.

H_2 temperature-programmed reduction (TPR) measurements of the promoted catalysts after calcination (Figure S4) show that the first peaks (associated with H_2 consumption because of the reduction of the Fe_2O_3 species to Fe_3O_4)[32] are located at 350–400 °C for the CMK-3- and OM-SiC-supported catalysts. Higher temperatures are required to initialize the reduction of the iron silicate species in the pore walls of the SBA-15-supported catalysts.

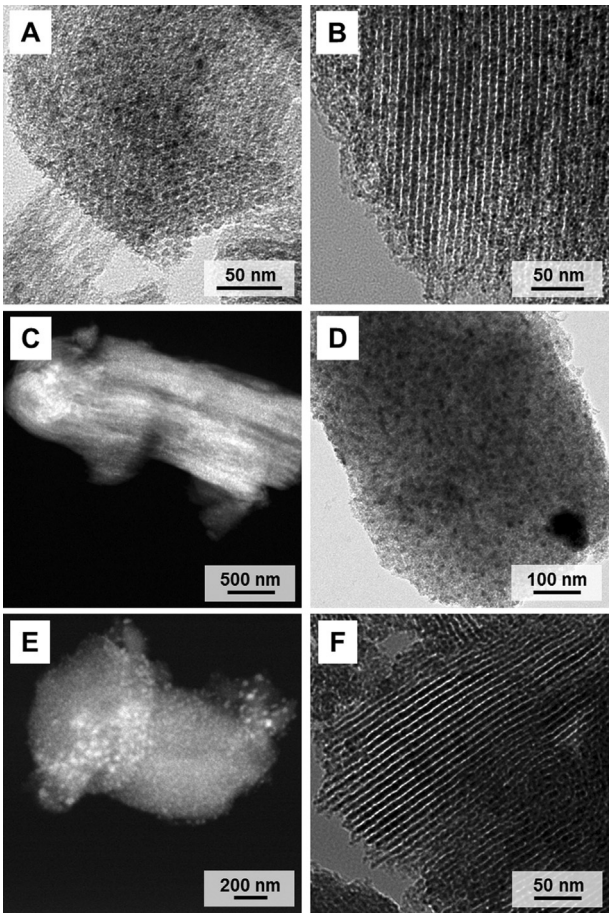

Figure 1. TEM and HAADF-STEM images of promoted Fe-based FTO catalysts supported on A–C) CMK-3, D and E) OM-SiC, and F) SBA-15 after calcination.

Mössbauer spectroscopy (Figure S5 and Table S3) of the calcined promoted catalysts shows the presence of predominantly Fe^{3+} species independent of the support material. In the OM-SiC-supported catalyst, 32% iron carbide species are detected after the decomposition of the iron citrate precursor at 500 °C under an inert atmosphere. After reduction at 350 °C in a diluted H_2 atmosphere, the Fe^{3+} species are reduced to Fe^{2+} in the CMK-3-supported catalyst, whereas in the OM-SiC-Fe-Na-S catalyst, the catalytically active Hägg carbide (χ-Fe_5C_2) is the dominant phase. In addition, metallic Fe as well as Fe^{2+} and Fe^{3+} species are present. No signs of activation are detected for the SBA-15 supported catalyst.

The catalytic properties of the Fe-based catalysts were first tested under FTO conditions of 350 °C, 1 bar, $H_2/CO = 1$, gas hourly space velocity (GHSV) = 1800 h^{-1}, which led to a CO conversion < 1.5%. Under these conditions, the extent of secondary reactions remains low and heat transfer limitations are minimized. The catalytic activity of the unpromoted CMK-3- and OM-SiC-supported catalysts is approximately one order of magnitude less than that of the promoted catalysts (Figure 2 A and Figure S6). In the presence of promoters, the different supports influence the properties of the Fe catalysts significantly

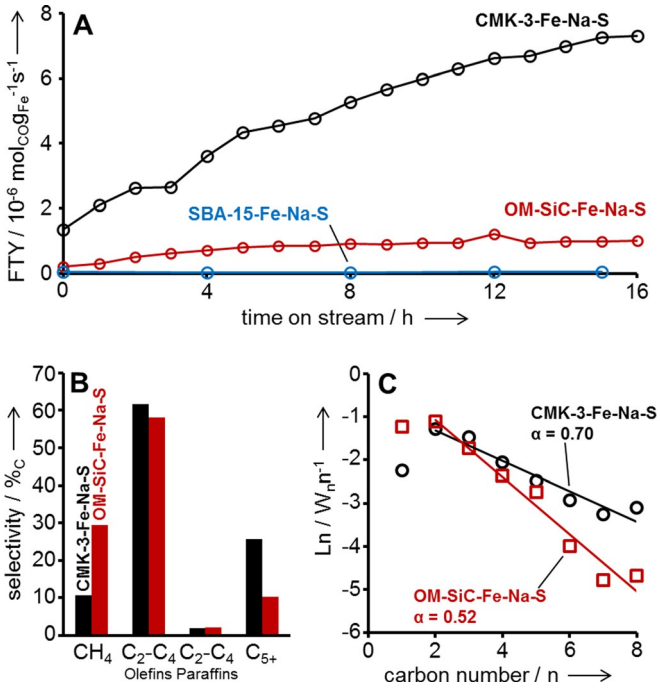

Figure 2. A) FTY over TOS for Na/S-promoted, Fe-based FTO catalysts under differential FTO conditions, B) product selectivity based on hydrocarbons produced, and C) ASF plots (C_1–C_8) as well as chain growth probability (α) based on the C_2–C_8 products of CMK-3- and OM-SiC-supported catalysts after 16 h TOS. Data obtained at GHSV = 1800 h^{-1}, $H_2/CO = 1$, $T = 350\,^{\circ}C$, $p = 1$ bar.

(Figure 2 and Table S4). As a result of the formation of iron silicate species, the activity of the SBA-supported catalyst is much lower than that of the non-oxidic supports. Even after 16 h time on stream (TOS), no formation of iron carbide species is observed by Mössbauer spectroscopy (Table S3). Notably, the Fe salt used can have a drastic influence on the Fe phase and dispersion, particularly on oxidic supports.[34] Previous studies have shown the possibility to obtain catalytically active iron carbide nanoparticles within the pore system of SBA-15 and other silica supports by using iron nitrate as the precursor.[9,35–37] In this study, we used iron citrate to illuminate the support effects on catalyst synthesis under similar conditions. Therefore, the low activity of the silica-supported catalyst reported here results from iron silicate formation during catalyst synthesis rather than from support effects on the promoter dispersion or the influence of the silica during catalyst operation.

In contrast, the promoted OM-SiC- and CMK-3-supported catalysts achieve a significant iron time yield (FTY) because of the presence of well-dispersed iron carbide nanoparticles and promotion by sodium and sulfur. However, the activity of the CMK-3-supported catalyst is notably higher than that of the OM-SiC-supported catalyst (Figure 2A). One reason for this is the more uniform dispersion and smaller diameter of the Fe particles in the pore system of CMK-3, which increases the number of active sites. Accordingly, Mössbauer spectroscopy after FTO shows a higher ratio of superparamagnetic Fe nanoparticles in the CMK-3-supported catalyst than that on OM-SiC (Table S3). After 16 h of TOS, both catalysts show a selectivity to C_2–C_4 olefins of ~60 $\%_C$ of the formed hydrocarbons (Figure 2B and Table S4). The CO_2 selectivity was not measured for FTO at 1 bar. The CMK-3-Fe-Na-S catalyst shows a low methane selectivity of ~11 $\%_C$ and a high selectivity of 25 $\%_C$ towards C_{5+} production, whereas OM-SiC-Fe-Na-S produces ~30 $\%_C$ of methane and only 10% C_{5+} molecules. Both catalysts exhibit high olefin/paraffin ratios of 31 (CMK-3-Fe-Na-S) and 29 (OM-SiC-Fe-Na-S) in the C_2–C_4 range. As the FTO process is based on a surface polymerization mechanism, the product distribution can be described by the Anderson–Schulz–Flory (ASF) model with the chain growth probability (α) as the key parameter.[1] The addition of Na as a promoter can increase α to lead to lower methane formation rates.[38] S can further decrease the methane formation by blocking the hydrogenation sites on the Fe catalyst.[8] In the ASF plots (Figure 2C) it can be seen that both catalysts show a methane selectivity below the predictions of the ASF model. The C_2–C_8 product distributions of both catalysts fit the ASF model. CMK-3-Fe-Na-S shows a higher chain growth probability ($\alpha = 0.70$) than OM-SiC-Fe-Na-S ($\alpha = 0.52$). In combination with its lower catalytic activity, this indicates that the Na promotion is less effective in case of the carbide-supported catalyst. This is likely caused by the presence of surface functional groups related to an oxidic passivation layer on the surface of amorphous silicon carbide with a high specific surface area (SSA).[29] In a similar way to SBA-15, this leads to the partial distribution of the Na ions on the support and to the less effective promotion of the Fe catalyst surface. Na promotion is more effective for the chemically inert and weakly interactive carbon support. S promotion is efficient in both cases, which can be seen from the methane formation below the ASF prediction and the high olefin/paraffin ratio in the C_2–C_4 range.

The influence of the concentration of S on the CMK-3-supported catalysts has been further investigated. The S content was varied from 0–3 wt% with respect to Fe. In the presence of S, the catalytic activities of the materials under differential conditions are very similar (Figure S7A and Table S4). The FTY of the CMK-3-supported catalyst without S is more than one order of magnitude lower that that with S. The absence of S also leads to an increase of the methane formation (28 $\%_C$) and to a lower olefin/paraffin ratio of 5.5 in the C_2–C_4 range (Figure S7B and Table S4). With increasing S loadings, the methane selectivity decreases slightly to values as low as 7 $\%_C$. At the same time, the lower olefin selectivities stay around 60%, whereas the C_{5+} production increases slightly. All the S-containing catalysts show a high chain growth probability in the C_2–C_8 area ($\alpha = 0.70$–0.74) because of the relatively high amount of Na. All of the S-promoted catalysts deviate significantly from the ASF product distribution because of the suppression of methane formation (Figure S7C). In combination with the weakly interacting CMK-3 support, this underlines the beneficial influence of the combination of Na/S promoters. CMK-3-Fe-Na-2S was further investigated in terms of long-term stability and it shows a stable FTY for more than 60 h TOS (Figure S8A). The selectivity for methane and lower olefins increases slightly with the increasing TOS (Figure S8B). The average

particle size increases to (9.23 ± 3.34) nm, but CMK-3-Fe-Na-2S does not show the growth of carbon filaments or the excessive aggregation of Fe particles after operation (Figure S8C).

The CMK-3-based FTO catalysts were also studied under industrially relevant FTO conditions (340 °C, 10 bar, $H_2/CO = 2$, GHSV = 9600 h^{-1}), which led to initial CO conversions of ~20%. The FTY values of the CMK-3-supported catalysts are significantly higher than those under FTO conditions at 1 bar. After an initial decrease of the catalytic activity, all catalysts show stable operation for up to 140 h of TOS at 10–12% CO conversion (Figure 3A, Table S5). The average particle size of the promoted catalysts increases within 140 h TOS to ~25–28 nm (Figure 3B and C and Figure S9). However, no excessive agglomeration or carbon fiber formation is observed, and the particles are still well dispersed over the CMK-3, which retains a highly ordered pore structure. These results prove the beneficial effect of the confinement of Fe particles within the internal pore system of ordered mesoporous materials. A recent study of FTO catalysts that use carbon nanofibers as supports under comparable conditions showed that particle growth is the predominant deactivation mechanism in the presence of promoters.[39] Significant particle growth up to average diameters of more than 50 nm was observed for fibrous supports with a less pronounced confinement effect. Under similar FTO conditions as applied to the CMK-3 catalysts, a promoted FTO catalyst supported on carbon black with larger and disordered mesopores shows a higher initial activity at comparable selectivity but a rapid decrease of activity (Figure S10). This shows the beneficial effect of the ordered mesoporous carbon support on the stability of FTO catalysts by confinement of the catalytically active Fe particles and thus limited growth. The simultaneously lower activity in comparison to the carbon black support shows that the encapsulation of small Fe nanoparticles into mesopores can lead to a decrease of the available catalyst surface and that the similar presence of an additional transport pore system would be beneficial to achieve high stability and activity at the same time.

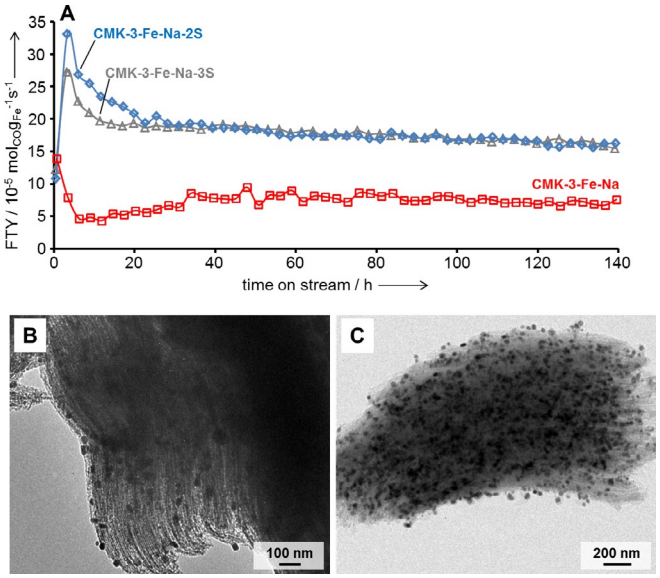

Figure 3. A) FTY over TOS for Na-promoted, CMK-3-supported, Fe-based FTO catalysts with different S contents at GHSV = 9600 h^{-1}, $H_2/CO = 2$, $T = 340$ °C, $p = 10$ bar. TEM images of B) CMK-3-Fe-Na-2S and C) CMK-3-Fe-Na-3S after 140 h TOS.

Similar to the studies under differential conditions, the presence of sulfur increases the catalytic activity, whereas the ratio of the promoter does not have a significant influence on the FTY (Figure 3A). Both S-containing catalysts show significantly higher C_2–C_4 olefin selectivities and lower methane and C_{5+} production than CMK-3-Fe-Na (Table S5), which indicates the efficiency of the S promoter even under industrially relevant conditions for up to 140 h TOS. Similar to the long-term FTO experiment with CMK-3-Fe-Na-2S at 1 bar, an increase of the methane and lower olefins selectivity as well as a decrease of the C_{5+} production is observed for the S-containing catalysts with increasing TOS (Table S5). As a result of the high WGS activity of the Fe catalysts, CO_2 selectivities of ~42%$_C$ are obtained at CO conversions around 20% at 10 bar. These values are comparable to those in previous reports.[8,34] The avoidance of excessive CO_2 formation is a point to tackle in future FTO research.

Conclusions

Several ordered mesoporous materials with comparable textural properties were used as model supports for Fe-based Fischer–Tropsch to olefins catalysts to gain a deeper understanding of the influence of the support chemistry on the catalyst synthesis, the effect of promoters, and the catalytic properties (Figure 4).

Small and well-dispersed Fe particles are present in CMK-3 supports. A broader distribution of the particle size and the formation of hardly reducible Fe species are observed for the OM-SiC and SBA-15 supports, respectively. Na and S promoters were most efficient for the carbon support with the lowest number of surface functional groups. An increase of the content of the sulfur promoter decreases the methane selectivity to $<8\%_C$, and $>60\%_C$ of lower olefins are present in the hydrocarbon products. The CMK-3-supported catalysts show a stable long-term operation, even for 140 h of time on stream under industrially relevant conditions, which shows the general promise of carbon supports for Fischer–Tropsch to olefins catalysts.

Experimental Section

Synthesis of the ordered mesoporous catalyst support materials

For the synthesis of SBA-15 silica with hexagonal pore ordering, the triblock copolymer Pluronic P123 (66.8 g; Sigma Aldrich) was dissolved in H_2O (1212 g) followed by the addition of concentrated aqueous HCl solution (38.6 g) and stirring overnight at 35 °C in a closed 2000 mL polypropylene bottle. Tetraethyl orthosilicate (143.6 g; 98%, Sigma Aldrich) was added to the solution, and the mixture was stirred at 35 °C for another 24 h. The white suspension was transferred to a Teflon-lined autoclave and treated hydrother-

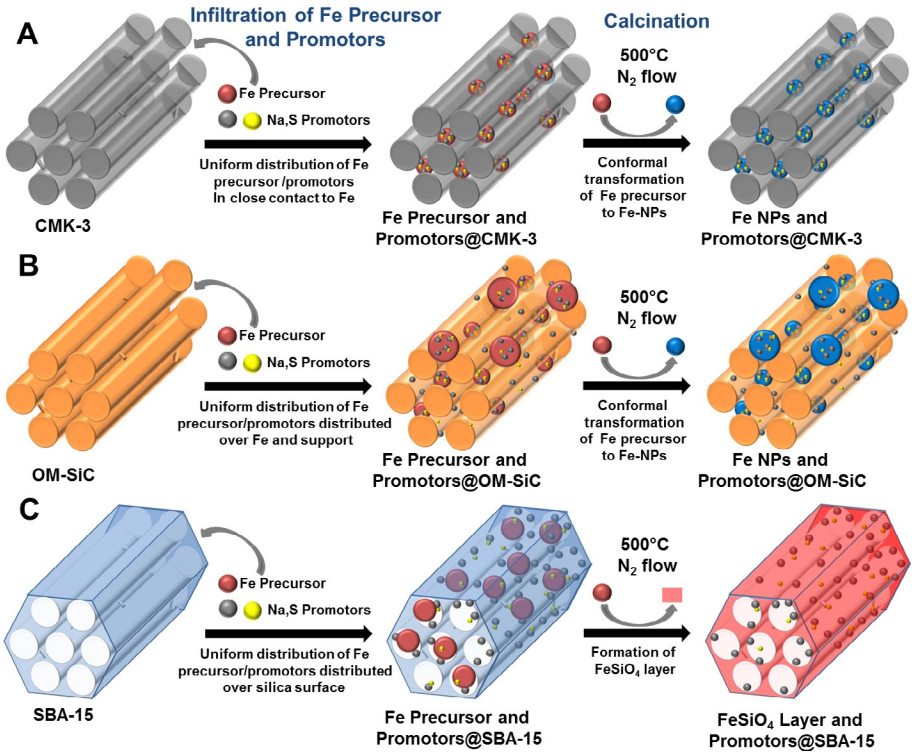

Figure 4. Ordered mesoporous materials as model supports for Fe-based FTO catalysts and their effects on the properties of the catalysts.

mally at 130 °C for 24 h followed by filtration and washing with deionized water/ethanol (~2000 mL, 1:1 by volume). After drying at 80 °C, SBA-15 was calcined at 550 °C for 5 h in a muffle furnace. The silica yield was ~38 g.

Ordered mesoporous SiC was synthesized by the nanocasting of SBA-15.[31] The silica template (2 g) was infiltrated in a mortar with a mixture of liquid allylhydridopolycarbosilane SMP-10 (2.1 mL; Starfire Systems) and *p*-divinylbenzene (0.5 mL) by incipient wetness impregnation (IWI). The pyrolysis of the SMP-10/SBA-15 composite was performed in a tubular furnace under a constant Ar flow at 800 °C for 2 h with a heating rate of 60 K h^{-1}. Silica dissolution was achieved by treating the SiC/SBA-15 composite material in a mixture of HF (35% solution in H_2O)/H_2O/EtOH, 1:1:1 by volume) for 3 h followed by filtration, washing with large amounts of ethanol, and drying at RT. The silicon carbide yield was ~1.5 g.

CMK-3 carbon material with a hexagonal mesopore arrangement was synthesized by mixing SBA-15 (2 g) with a solution of sucrose (2.5 g) and concentrated H_2SO_4 (280 mg) in H_2O (10 mL) in a porcelain dish. The carbohydrate was polymerized by heating the mixture to 100 °C for 6 h and to 160 °C for another 6 h in air. Subsequently, the material was impregnated again with a solution of sucrose (1.6 g) and concentrated H_2SO_4 (180 mg) in H_2O (10 mL), again followed by heating to 100 and 160 °C. Carbonization was performed in a tubular furnace under a constant Ar flow at 900 °C for 2 h with a heating rate of 150 K h^{-1}. Silica dissolution was performed similarly to that of the ordered mesoporous SiC described above. The carbon yield was ~1.1 g.

Synthesis of the supported Fe catalysts

To load Fe and the Na/S promoters, the support materials (270 mg) were impregnated with an aqueous solution (400 μL) of ammonium iron(III) citrate (187 mg; Fluka, 14.5–16% Fe), sodium citrate dihydrate (38 mg; 99%, Sigma Aldrich), and iron sulfate heptahydrate (2.6 mg; 99%, Sigma Aldrich) by the IWI method to achieve a loading of 10 wt% Fe with respect to the support and 30 wt% Na and 1 wt% S with respect to Fe. Unpromoted Fe catalysts were prepared by the infiltration of an aqueous solution that contained only ammonium iron(III) citrate. For the preparation of CMK-3-supported catalysts with different contents of S, the amount of iron sulfate heptahydrate was increased or no sulfate was added. After impregnation, the catalysts were dried overnight at 120 °C under static air followed by subsequent calcination at 500 °C for 2 h in a tubular furnace under N_2 flow (heating rate = 2 K min^{-1}). The catalysts are labeled as Support material-Fe-Na-S (promoted) and Support material-Fe (unpromoted). The various contents of S in the promoted CMK-3-supported catalysts are labeled with either the absence of the suffix (no sulfur), or -S, -2S, -3S (1, 2, or 3 wt% theoretical S with respect to Fe, respectively). The reference catalyst was treated in the same way as the CMK-3-Fe-Na-S catalyst. Carbon black (SSA = 1125 $m^2 g^{-1}$, V_{pore} = 1.55 $cm^3 g^{-1}$) was used as the support.

Catalyst characterization

N_2 physisorption isotherms were measured at −196 °C by using a Quntachrome Quadrasorb apparatus. Before all measurements, samples were degassed under vacuum at 150 °C. The SSA values were calculated with the multipoint Brunauer–Emmett–Teller (MP-BET) equation ($0.05 < p/p_0 < 0.2$). Total pore volumes were calculated from the volume of adsorbed N_2 at $p/p_0 = 0.965$. PSD values were calculated with the quenched solid density functional theory (QSDFT) method (based on the adsorption branch) for N_2 at −196 °C on carbon surfaces with cylindrical pore geometry in case of OM-SiC and CMK-3. To calculate the PSD of the SBA-15 support,

the nonlocal density functional theory (NLDFT) method (based on the adsorption branch) for N_2 at −196 °C on silica surfaces with cylindrical pore geometry was applied. Micropore volumes (MPV) were calculated from the cumulative DFT pore volumes at a diameter of 2 nm.

Transmission ^{57}Fe Mössbauer absorption spectra were collected in situ at 27 °C by using a conventional constant-acceleration spectrometer using a ^{57}Co(Rh) source. Velocity calibration was performed using an α-Fe foil. The Mössbauer spectra were fitted using the Mosswinn 4.0 program. TEM and high-angle annular dark-field (HAADF) scanning transmission electron microscopy (STEM) measurements were performed by using an FEI Tecnai 20 FEG instrument operated at 200 kV. Before the measurements, the samples were ground into fine powders, dispersed in ethanol, sonicated for ~30 s, and drop-casted on a carbon-coated copper TEM grid. ICP-OES measurements were performed by using a SPECTRO ARCOS ICP-OES instrument. The determined contents of Na and S could have an experimental error >10% because of their low concentration. XRD measurements were performed by using a Bruker D2 PHASER with a $CuK_{\alpha1}$ radiation source ($\lambda = 0.154$ nm). H_2-TPR was conducted by heating 50–60 mg of the calcined catalysts to 800 °C at a rate of 5 K min^{-1} in 50 mL min^{-1} of a gas mixture of 5% H_2 in Ar by using a Micromeritics Autochem II 2920 Chemisorption Analyzer.

Catalytic tests at 1 bar

Catalytic testing of the Fe-based FTO catalysts under differential conditions was performed at 1 bar, 350 °C, H_2/CO ratio of 1, and a GHSV of 1800 h^{-1}. The FTO reaction was performed at low CO conversions (<1.5%) to ensure differential operation to minimize the extent of secondary reactions and heat transfer limitations. Calcined catalysts were sieved to a particle size fraction of 75–212 μm. The catalyst (200 μL) was diluted with silicon carbide (200 μL; 212–425 μm) and transferred to a plug-flow fixed-bed reactor. Catalysts were reduced before reaction for 2 h at 350 °C (heating rate 5 K min^{-1}) in 15 mL min^{-1} of a H_2/He mixture (1:2 by volume) followed by cooling to 290 °C. Then, the flow was changed to 6 mL min^{-1} of a H_2/CO syngas mixture (1:1 by volume) to allow carbide formation under mild conditions for 1 h. For the FTO reaction, the temperature was increased to 350 °C again (TOS = 0 h). The C_1–C_{16} products were analyzed by using an online gas chromatograph Varian CP3800 equipped with a flame ionization detector (FID). The product selectivity [$\%_C$] was calculated as the equivalent of carbon atoms present in a product fraction in relation to the total carbon atoms present in the hydrocarbons. The CO_2 selectivity was not measured. The activity of the catalysts is expressed as FTY in moles of converted CO to hydrocarbons per gram of Fe per second. The experimental error of the selectivities at measurements with very low CO conversions <0.2% is more significant than that of the catalyst samples with a higher CO conversion.

Catalytic tests at 10 bar

Catalytic testing of the Fe-based FTO catalysts under industrially relevant conditions was performed in a 16-reactor catalytic testing setup (Flowrence, Avantium) at 10 bar, 340 °C, H_2/CO ratio of 2, and a GHSV of 9600 h^{-1}. The FTO reaction was performed at medium CO conversions (~20% initial conversion). Calcined catalysts were sieved to a particle size fraction of 75–212 μm. The catalyst (50 μL) was diluted with silicon carbide (50 μL; 212–425 μm) and transferred to a plug-flow fixed-bed reactor. The catalysts were dried in a flow of He at 280 °C for 20 min at 3 bar and then reduced in situ in a flow of H_2/CO (2:1 by volume) at 280 °C and 3 bar for 10 min. Then, the temperature was increased to 340 °C (heating rate 2 K min^{-1}) and after 10 min, the pressure was increased to 10 bar (TOS = 0 h). The products were analyzed by using online GC (Agilent 7890A). The permanent gases and CO_2 were separated by using a ShinCarbon ST (#19043) column and quantified against He as an internal standard using a thermal conductivity detector (TCD). CO conversions were calculated as $X_{CO} = (mol_{CO,in} - mol_{CO,out})/mol_{CO,in}$. Hydrocarbons ($C_1$–$C_9$) were separated by using an Agilent J&W PoraBOND Q column, detected by using an FID and quantified against the TCD signal of the internal standard He. Selectivities to CO_2 were calculated from the converted CO and the corresponding yields as $S_{CO_2} = Y_{CO_2}/(mol_{CO,in} - mol_{CO,out})$. As for the measurements at 1 bar, product selectivity in the formed hydrocarbons was calculated on a carbon atom basis. At the end of the catalytic tests, the reactors were cooled to RT under a flow of He.

Acknowledgements

M.O. acknowledges financial support from the Postdoc-Program of the German Academic Exchange Service (DAAD). We thank Helen de Waard (Utrecht University) for the IPC-OES measurements and Prof. Dr. Stefan Kaskel (TU Dresden) for providing the OM-SiC material and physisorption data.

Keywords: Fischer–Tropsch synthesis · heterogeneous catalysis · mesoporous materials · promoters · surface chemistry

[1] H. M. Torres Galvis, K. P. de Jong, *ACS Catal.* **2013**, *3*, 2130.
[2] X. Zhou, J. Ji, D. Wang, X. Duan, G. Qian, D. Chen, X. Zhou, *Chem. Commun.* **2015**, *51*, 8853.
[3] X. Chen, D. Deng, X. Pan, Y. Hu, X. Bao, *Chem. Commun.* **2015**, *51*, 217.
[4] C. Wang, P. Zhai, Z. Zhang, Y. Zhou, J. Ju, Z. Shi, D. Ma, R. P. S. Han, F. Huang, *Part. Part. Syst. Charact.* **2015**, *32*, 29.
[5] B. Sun, K. Xu, L. Nguyen, M. Qiao, F. F. Tao, *ChemCatChem* **2012**, *4*, 1498.
[6] C. López, A. Corma, *ChemCatChem* **2012**, *4*, 751.
[7] S. Abelló, D. Montané, *ChemSusChem* **2011**, *4*, 1538.
[8] H. M. Torres Galvis, A. C. J. Koeken, J. H. Bitter, T. Davidian, M. Ruitenbeek, A. I. Dugulan, K. P. de Jong, *J. Catal.* **2013**, *303*, 22.
[9] K. Cheng, V. V. Ordomsky, B. Legras, M. Virginie, S. Paul, Y. Wang, A. Y. Khodakov, *Appl. Catal. A* **2015**, *502*, 204.
[10] H. M. Torres Galvis, J. H. Bitter, C. B. Khare, M. Ruitenbeek, A. I. Dugulan, K. P. de Jong, *Science* **2012**, *335*, 835.
[11] V. P. Santos, T. A. Wezendonk, J. J. D. Jaén, A. I. Dugulan, M. A. Nasalevich, H.-U. Islam, A. Chojecki, S. Sartipi, X. Sun, A. A. Hakeem, A. C. J. Koeken, M. Ruitenbeek, T. Davidian, G. R. Meima, G. Sankar, F. Kapteijn, M. Makkee, J. Gascon, *Nat. Commun.* **2015**, *6*, 6451.
[12] H. Schulz, *Catal. Today* **2014**, *228*, 113.
[13] Z. H. Chonco, A. Ferreira, L. Lodya, M. Claeys, E. J. Van Steen, *J. Catal.* **2013**, *307*, 283.
[14] S. Li, A. Li, S. Krishnamoorthy, E. Iglesia, *Catal. Lett.* **2001**, *77*, 197.
[15] M. Saglam, *Ind. Eng. Chem. Res.* **1989**, *28*, 150.
[16] M. C. Ribeiro, G. Jacobs, B. H. Davis, D. C. Cronauer, A. J. Kropf, C. L. Marshall, *J. Phys. Chem. C* **2010**, *114*, 7895.
[17] A. C. J. Koeken, H. M. Torres Galvis, T. Davidian, M. Ruitenbeek, K. P. de Jong, *Angew. Chem. Int. Ed.* **2012**, *51*, 7190; *Angew. Chem.* **2012**, *124*, 7302.
[18] M. Casavola, J. Hermannsdörfer, N. de Jonge, A. I. Dugulan, K. P. de Jong, *Adv. Funct. Mater.* **2015**, *25*, 5309.
[19] J.-D. Xu, K.-T. Zhu, X.-F. Weng, W.-Z. Weng, C.-J. Huang, H.-L. Wan, *Catal. Today* **2013**, *215*, 86.

[20] D. Fu, W. Dai, X. Xu, W. Mao, J. Su, Z. Zhang, B. Shi, J. Smith, P. Li, J. Xu, Y.-F. Han, *ChemCatChem* **2015**, *7*, 752.
[21] K. Cheng, M. Virginie, V. V. Ordomsky, C. Cordier, P. A. Chernavskii, M. I. Ivantsov, S. Paul, Y. Wang, A. Y. Khodakov, *J. Catal.* **2015**, *328*, 139.
[22] J. Lu, L. Yang, B. Xu, Q. Wu, D. Zhang, S. Yuan, Y. Zhai, X. Wang, Y. Fan, Z. Hu, *ACS Catal.* **2014**, *4*, 613.
[23] W. Chen, Z. Fan, X. Pan, X. Bao, *J. Am. Chem. Soc.* **2008**, *130*, 9414.
[24] A. Y. Khodakov, A. Griboval-Constant, R. Bechara, V. L. Zholobenko, *J. Catal.* **2002**, *206*, 230.
[25] K.-S. Ha, G. Kwak, K.-W. Jun, J. Hwang, J. Lee, *Chem. Commun.* **2013**, *49*, 5141.
[26] Z. Sun, B. Sun, M. Qiao, J. Wei, Q. Yue, C. Wang, Y. Deng, S. Kaliaguine, D. Zhao, *J. Am. Chem. Soc.* **2012**, *134*, 17653.
[27] D. Zhao, J. Feng, Q. Huo, N. Melosh, G. Fredrickson, B. Chmelka, G. Stucky, *Science* **1998**, *279*, 548.
[28] S. Jun, S. H. Joo, R. Ryoo, M. Kruk, M. Jaroniec, Z. Liu, T. Ohsuna, O. Terasaki, *J. Am. Chem. Soc.* **2000**, *122*, 10712.
[29] P. Krawiec, D. Geiger, S. Kaskel, *Chem. Commun.* **2006**, 2469.
[30] A. Silvestre-Albero, E. O. Jardim, E. Bruijn, V. Meynen, P. Cool, A. Sepulveda-Escribano, J. Silvestre-Albero, F. Rodriguez-Reinoso, *Langmuir* **2009**, *25*, 939.
[31] M. Oschatz, L. Borchardt, S. Rico-Francés, F. Rodríguez-Reinoso, S. Kaskel, J. Silvestre-Albero, *Langmuir* **2013**, *29*, 8133.
[32] H. J. Schulte, B. Graf, W. Xia, M. Muhler, *ChemCatChem* **2012**, *4*, 350.
[33] R. P. Mogorosi, N. Fischer, M. Claeys, E. Van Steen, *J. Catal.* **2012**, *289*, 140.
[34] H. M. Torres Galvis, A. C. J. Koekena, J. H. Bitter, T. Davidian, M. Ruitenbeek, A. I. Dugulan, K. P. de Jong, *Catal. Today* **2013**, *215*, 95.
[35] K. Cheng, V. V. Ordomsky, M. Virginie, B. Legras, P. A. Chernavskii, V. O. Kazak, C. Cordier, S. Paul, Y. Wang, A. Y. Khodakov, *Appl. Catal. A* **2014**, *488*, 66.
[36] P. A. Chernavskii, V. O. Kazak, G. V. Pankina, V. V. Ordomsky, A. Y. Khodakov, *ChemCatChem* **2016**, *8*, 390.
[37] H. Yang, Q. Lu, F. Gao, Q. Shi, Y. Yan, F. Zhang, S. Xie, B. Tu, D. Zhao, *Adv. Funct. Mater.* **2005**, *15*, 1377.
[38] X. An, B. S. Wu, H. J. Wan, T. Z. Li, Z. C. Tao, H. W. Xiang, Y. W. Li, *Catal. Commun.* **2007**, *8*, 1957.
[39] J. Xie, H. M. Torres Galvis, A. C. J. Koeken, A. Kirilin, A. I. Dugulan, M. Ruitenbeek, K. P. de Jong, *ACS Catal.* **2016**, *6*, 4017.

Received: April 26, 2016
Published online on August 5, 2016